

Felina Schütz | Gerd Winterleitner | Ernst Huenges

# Geothermal exploration in a sedimentary basin

New continuous temperature data and  
physical rock properties from northern Oman

Suggested citation referring to the original publication:  
Geothermal Energy 6 (2018) 5  
DOI <https://doi.org/10.1186/s40517-018-0091-6>  
ISSN (online) 2195-9706

Postprint archived at the Institutional Repository of the Potsdam University in:  
Postprints der Universität Potsdam  
Mathematisch-Naturwissenschaftliche Reihe ; 934  
ISSN 1866-8372  
<https://nbn-resolving.org/urn:nbn:de:kobv:517-opus4-459317>  
DOI <https://doi.org/10.25932/publishup-45931>



RESEARCH

Open Access



# Geothermal exploration in a sedimentary basin: new continuous temperature data and physical rock properties from northern Oman

Felina Schütz<sup>1\*</sup> , Gerd Winterleitner<sup>1,2</sup> and Ernst Huenges<sup>1</sup>

\*Correspondence:

fschuetz@gfz-potsdam.de

<sup>1</sup> Section 6.2 Geothermal Energy Systems, Helmholtz Centre Potsdam-GFZ

German Research

Centre for Geoscience,

Telegrafenberg,

14473 Potsdam, Germany

Full list of author information is available at the end of the article

## Abstract

The lateral and vertical temperature distribution in Oman is so far only poorly understood, particularly in the area between Muscat and the Batinah coast, which is the area of this study and which is composed of Cenozoic sediments developed as part of a foreland basin of the Makran Thrust Zone. Temperature logs (T-logs) were run and physical rock properties of the sediments were analyzed to understand the temperature distribution, thermal and hydraulic properties, and heat-transport processes within the sedimentary cover of northern Oman. An advective component is evident in the otherwise conduction-dominated geothermal play system, and is caused by both topography and density driven flow. Calculated temperature gradients (T-gradients) in two wells that represent conductive conditions are 18.7 and 19.5 °C km<sup>-1</sup>, corresponding to about 70–90 °C at 2000–3000 m depth. This indicates a geothermal potential that can be used for energy intensive applications like cooling or water desalination. Sedimentation in the foreland basin was initiated after the obduction of the Semail Ophiolite in the late Campanian, and reflects the complex history of alternating periods of transgressive and regressive sequences with erosion of the Oman Mountains. Thermal and hydraulic parameters were analyzed of the basin's heterogeneous clastic and carbonate sedimentary sequence. Surface heat-flow values of 46.4 and 47.9 mW m<sup>-2</sup> were calculated from the T-logs and calculated thermal conductivity values in two wells. The results of this study serve as a starting point for assessing different geothermal applications that may be suitable for northern Oman.

**Keywords:** Continuous temperature logging, Physical rock properties, Sedimentary basin, Geothermal applications in Oman

## Introduction

### Background

Geothermal systems currently under exploitation are found in a number of geological environments, where temperatures and depths of the reservoirs vary accordingly. Many high-temperature (> 180 °C) hydrothermal systems are associated with recent volcanic activity and are found near plate tectonic boundaries (e.g., subduction zones, rift systems, oceanic spreading centers or transform margins), or at crustal and mantle hot spot

anomalies. Such systems cannot be expected in Oman, but do occur in other parts of the Arabian Peninsula. In Saudi Arabia and Yemen several active volcanos are associated with the Afar Plume and the recent opening of the Red Sea (Chang and Van der Lee 2011). Intermediate- (100–180 °C) and low-temperature (<100 °C) systems in continental settings are either linked to above-normal heat production and increased terrestrial heat flow through radioactive isotope decay, or to aquifers charged by hot water originating from circulation along deep (crustal-scale) fault zones (Huenges 2010).

Our study focused on the sedimentary infill of the foreland basin north of the Oman Mountains, which consists of Cenozoic sediments. The main aim of this study is to understand the temperature distribution in the subsurface and the physical rock properties of the carbonate and clastic sediments that accumulated after the obduction of the Semail Ophiolite complex during the late Cretaceous time. We evaluated temperature logs (T-logs) in terms of advective and conductive components to determine a geothermal gradient representative for the area. We further derived heat flow values for two well locations and used these data to calculate the temperature at depth as addition to the well logs.

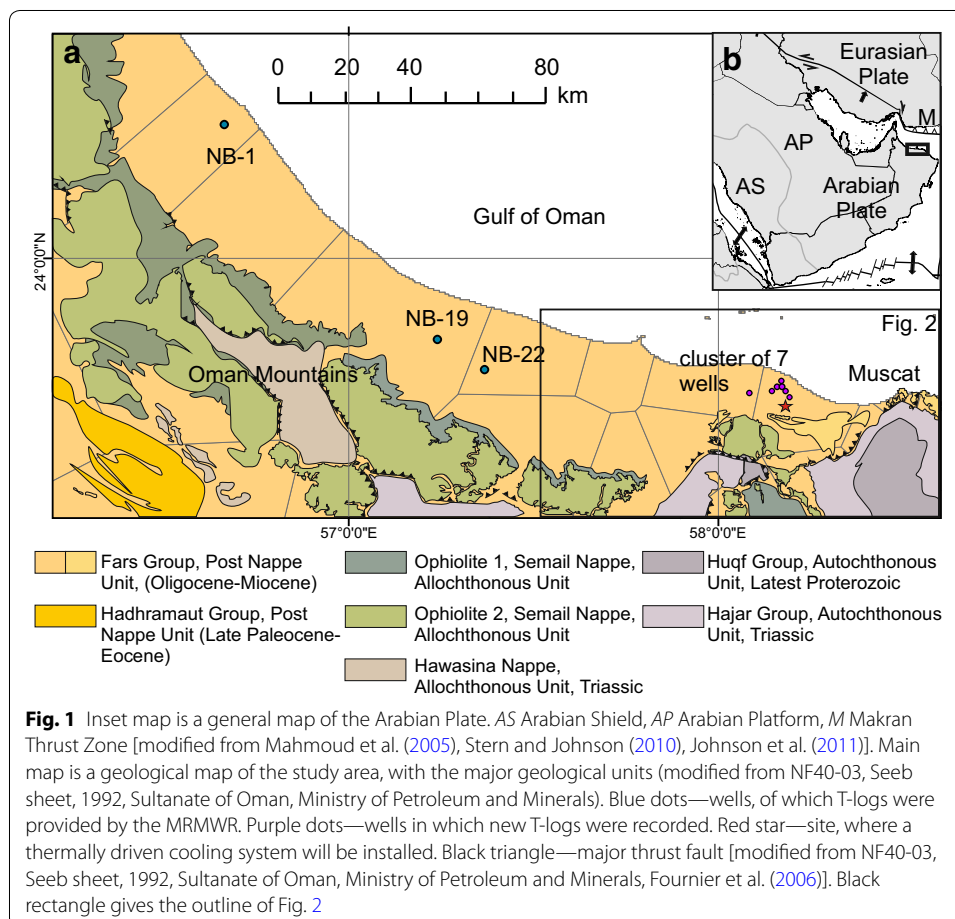
#### **Status quo of geothermal use in Oman and its surroundings**

Geothermal energy is currently not represented in the national energy mix of Oman and only plays a very minor role in the Arabian Peninsula in general. In the whole region a large percentage of the energy consumption is used for cooling. In Oman 50% of the residential power supply is only used for residential cooling (Sweetnam et al. 2014) in Saudi Arabia even 80% and the average for the whole Gulf Cooperation Council (GCC), consisting of Bahrain, Kuwait, Oman, Qatar, Saudi Arabia, and the United Arab Emirates, is 40–50% (Lashin et al. 2015). The electricity demand will rise in the GCC by 7–8% per year on average; in the smallest and fastest-growing economies, demand will grow even faster (GCC 2010). The electricity sector in Oman is primarily based on natural gas (97.5%) and diesel (2.5%, Authority for Electricity Regulation, Oman). The same applies to the other GCC countries, which all fall in the top 25 countries of carbon dioxide emissions per capita (Reiche 2010). Geothermal energy could significantly contribute to a greener energy mix, especially in countries in possession of high-temperature and intermediate temperature hydrothermal systems, like Saudi Arabia and the Yemen. The usage of thermally driven cooling could significantly help to lower the energy demand in this sector. Thermally driven cooling requires temperatures of 70–100 °C. The energy for sustainable cooling supply can be developed from solar and geothermal sources. Solar heat supply is fluctuating, whereas geothermal heat can provide base load heat supply. The results of this study show that the target temperatures can be reached in around 2000 m depth. Fault structures which exist in the contact zone between the Tertiary sedimentary sequence and the Semail Ophiolite, correlated with hot springs, constitute a potential setting for drilling.

#### **Research collaboration and implication of the study**

The present study is part of a research collaboration between The Research Council (TRC) of the Sultanate of Oman and the German Research Centre for Geosciences (GFZ), which seeks to develop a cooling system driven by renewables. Both geothermal

and solar energy are considered as potential options to deliver the hot water required to drive an absorption chiller. A prototype of this cooling system will be installed at the study site 40 km west of Muscat to cool one institute building of the TRC (Fig. 1). The temperature distribution with depth is an important parameter for evaluating the potential of geothermal energy as driving heat for an absorption chiller and is also required for the planning of other shallow geothermal installations. One example of a shallow geothermal system is underground storage where energy, in the form of hot or cold water, is temporarily stored in the subsurface and recovered when needed. These systems are increasingly used in Europe, and are also of interest for countries in the sun-belt, especially in combination with solar, wind or any other existing fluctuating energy source to utilize excess and surplus energies as auxiliary energy back-up systems during peak demand times. A further challenge of the region is the rejection of process waste heat during hot summer months. The ambient air temperature of Oman is too high to efficiently reject the heat to the surrounding environment. The conventional method in a climate like Muscat would be to use a cooling tower, but they become inefficient when the ambient temperature and humidity rise up in summer. A more energy-efficient approach is to inject the process waste heat to the subsurface, where conditions are cooler and more stable. Over the course of the year, the ground temperature only varies



slightly at a fixed depth and during the hot summer months when temperature in Muscat can rise to 47 °C (Directorate General of Meteorology, Oman, PACA) the subsurface temperature is significantly lower. It is therefore possible to reject the process waste heat into intermediate aquifers, where minimum temperatures were measured. To plan and simulate such an application the temperature gradient (T-gradient) and the physical rock properties of the underground are required. The data generated in this study serve as background for further analysis of an intelligent utilization of the subsurface in combination with a thermally driven cooling system at the study site, 40 km west of Muscat.

### **Geological setting**

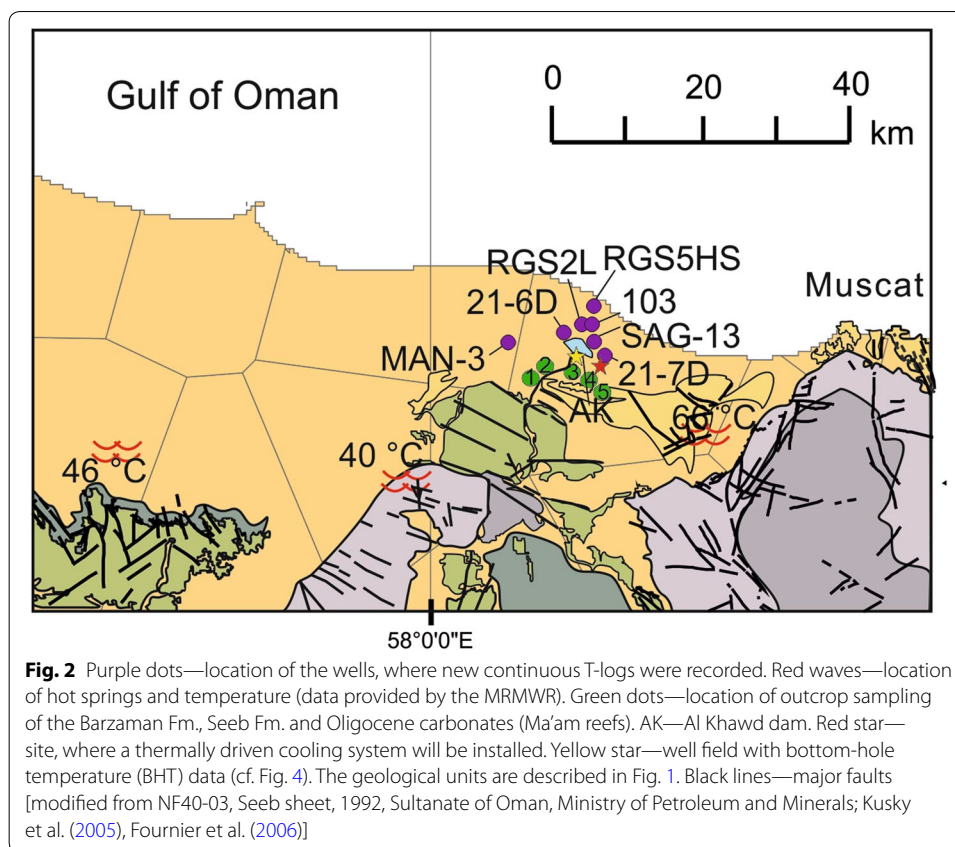
Oman is located at the south-eastern margin of the Arabian Plate, which can be divided into the Arabian Shield and the Arabian Platform. The Arabian Shield comprises juvenile continental crust of mainly Neoproterozoic age and is partly covered by younger sediments (Stern and Johnson 2010). The Arabian Platform, in contrast, is mostly covered by Phanerozoic sediments, which dominate the western part of the Arabian Plate (see inset of Fig. 1). The Phanerozoic cover is up to 10 km thick and defines the large stable platform of eastern Arabia. During late Cretaceous times a subduction zone and island arc complex developed in the Tethyan Ocean, whose remnants now constitute the Gulf of Oman. The Arabian Plate moved progressively northwards and early phases of collision between the Arabian continent and the Iranian block (Eurasian Plate) started. During the subduction process a thrust slice of the Tethys Ocean floor was obducted on the NE margin of the Arabian Platform, to form the Semail Ophiolite, which nowadays represent the Oman Mountains (Alsharhan 2014).

Five tectonic sequences are recognized in Oman. They are comprised of the following units: (1) Pre-Permian (Huqf Group), (2) the Hajar Supergroup (Permian to Cretaceous sediments), (3) the Allochthonous Sequence (Semail Nappe and Hawasina Nappe), (4) the Hadhramaut Group, and (5) the Fars Group. The latter two are part of the neoautochthonous sedimentary cover (Al-Lazki and Barazangi 2002).

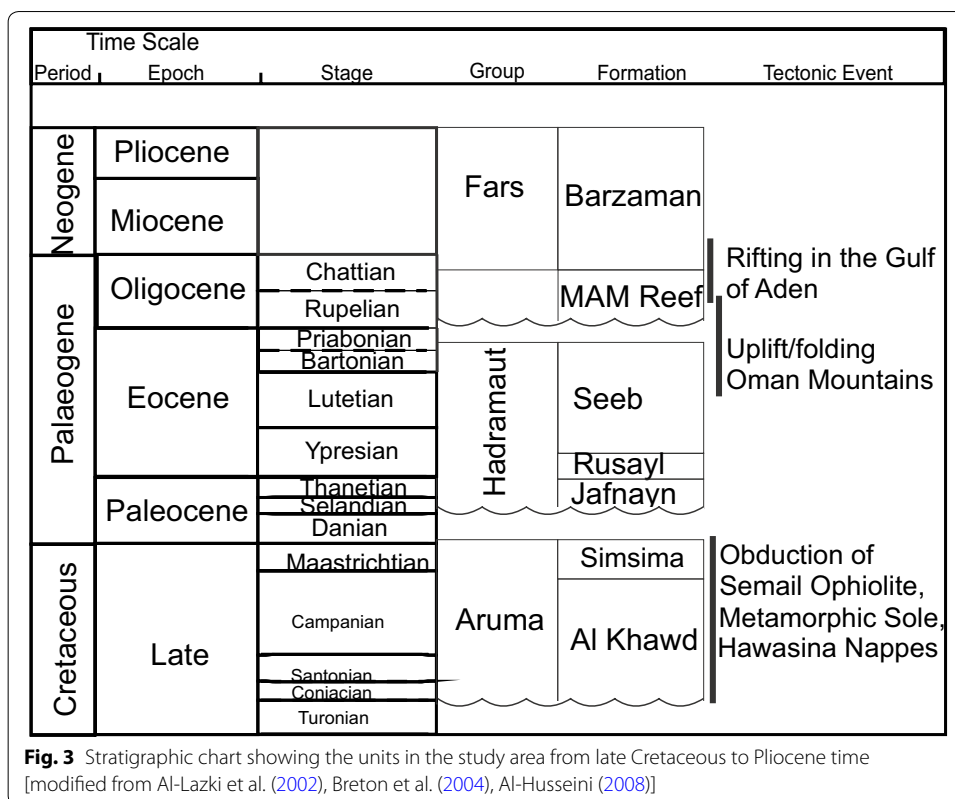
The ophiolite sequence is divided into a unit of cumulate layered gabbro (Ophiolite 1), and a unit composed of harzburgite with minor lherzolite and dunite (Ophiolite 2). The Hadhramaut Group and the Fars Group are an assemblage of late Maastrichtian and Tertiary sediments, unconformably deposited on top of the allochthonous units (Stern and Johnson 2010) and forming the neoautochthonous sedimentary cover (termed post nappe unit in Fig. 1). Our study area is located in the Al Khawd Fan aquifer system (see Fig. 2), which is part of the neoautochthonous sedimentary cover between Muscat and the Batinah coast and thus part of the convergence zone between the Arabian and Eurasian Plates. In the following paragraphs the stratigraphic and structural characteristics of the area are described.

### **Post-obduction sequences**

Development of the foreland basin started with the obduction of the Semail Ophiolite complex onto the Arabian Platform during the late Campanian. The first sediments deposited in the evolving basin were siliciclastic sediments originating from the unroofing of the emergent proto-Oman Mountains (Al Khawd Formation). They unconformably rest on the ophiolitic basement and are composed of fluvialite,



and localised beach to fan delta deposits. The boundary to the overlying Simsima (shallow shelf carbonate) Formation is described for the area as conformable and elsewhere a non-sequence is present (Nolan et al. 1990). The late Palaeocene to early-Eocene shallow-marine carbonates of the Jafnayn Formation were deposited on top of a major regional unconformity, separating Paleogene and Cretaceous strata in the central Oman Mountains (Özcan et al. 2015; Tomás et al. 2016). Subsequently, the shale and fine-grained limestones of the Rusayl Formation (early-Eocene age) were deposited in a fluvial and lagoonal environment (Dill et al. 2007). A marine transgression during the middle Eocene resulted in the development of a carbonate platform which is represented in the stratigraphic succession as the Seeb Formation (Fig. 3). Sediments were deposited on a storm-influenced carbonate ramp with well-defined inner, mid to outer ramp facies belts, and a general fining-upward trend. Deposition of the Seeb carbonates terminated at the end of the Eocene with the emersion of the Arabian Platform due to the opening of the Red Sea. Marine carbonate-dominated sedimentation resumed during the Oligocene (Ma'am platform reefs) followed by the mixed carbonate siliciclastic Barzaman Formation which developed as an alluvial fan system during Miocene to Pliocene times (Fig. 3). The latter started with the emergence and subsequent erosion of the Oman Mountains (Al-Lazki and Barazangi 2002). Nolan et al. (1990) described the general stratigraphy and depositional systems of the post-obduction sediments accumulated in the Batinah coast area in detail.



**Structural characteristics**

Faults, fracture zones and karst zones in carbonates are of special interest for geothermal exploitation. In the Batinah coastal plain, compression resumed after a late Cretaceous to Paleogene extensional phase that followed obduction of the ophiolite. The extensional phase caused large-scale normal faulting in the northeast Oman margin. Extensional tectonics were recognized from the observation of normal faults displacing the post-nappes sedimentary deposits against the autochthonous series or the ophiolites; for example at the Batinah coast and the Rusayl Embayment (Fournier et al. 2006). Convergence between the north Oman margin and the Zagros–Makran appears to have been re-established by the Eocene (Coleman 1981; Mann et al. 1990). The autochthonous sedimentary cover, allochthonous nappe complex, and the neoautochthonous sedimentary cover were further affected in the axial zone and the foreland basin of the Oman Mountains by large-scale folding, short-distance thrusting, and uplift (Searle et al. 1983; Michard et al. 1984; Searle 1985; Poupeau et al. 1998; Mount et al. 1998; Al-Lazki and Barazangi 2002; Fournier et al. 2006). Their broad structural style indicates that shortening was minor. Hence, the onset of compression in the Oman Mountains was either synchronous with late Oligocene to early Miocene rifting in the Gulf of Aden, or started immediately thereafter. Compressional deformation continued until the Pliocene and is recorded in the Mio-Pliocene deposits of the Barzaman Formation (Fournier et al. 2006).



## Methods

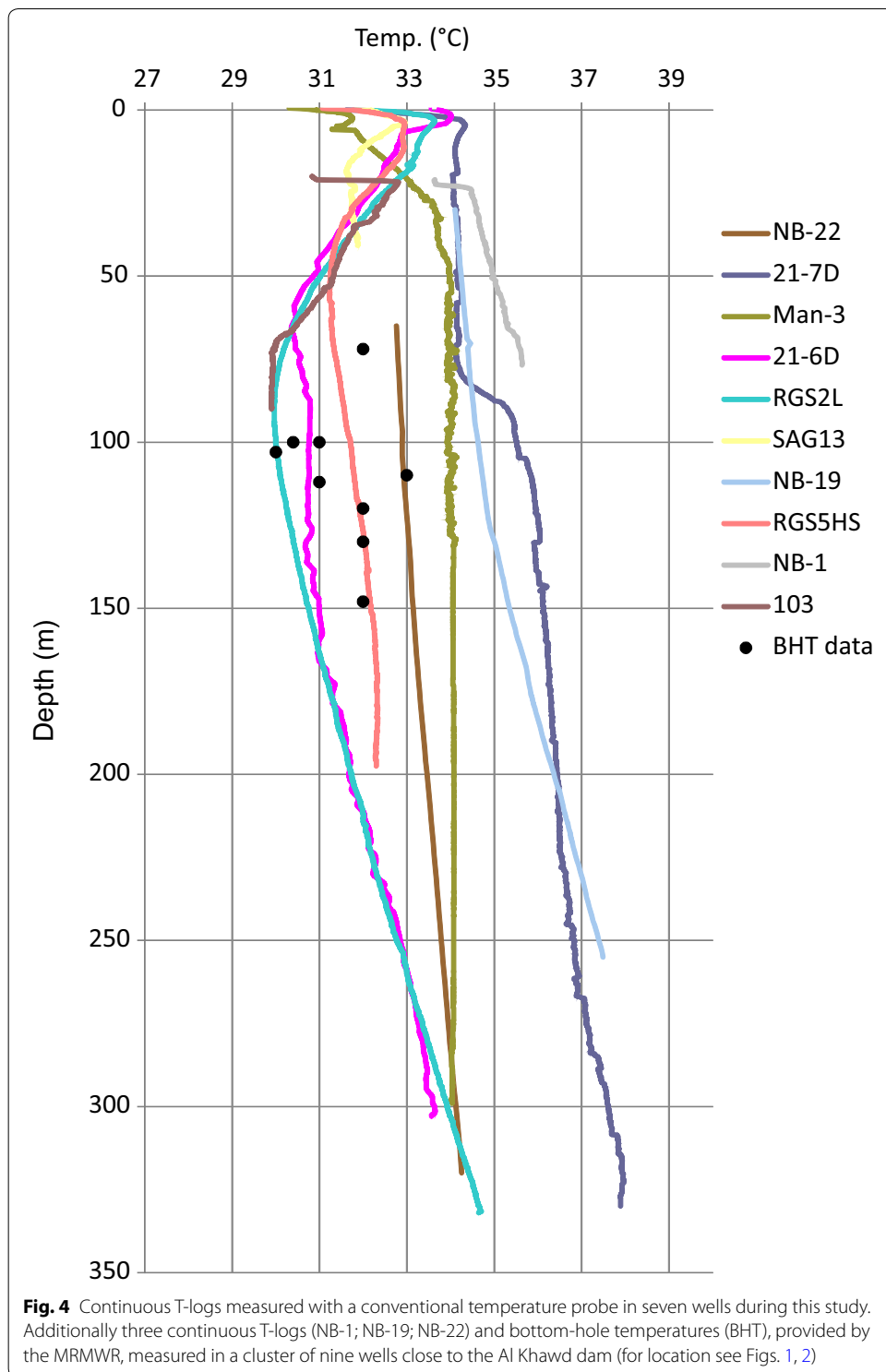
### Physical rock properties

Due to the lack of suitable core material we collected outcrop samples of the sedimentary succession in a field campaign (see Fig. 2 for location details). The outcrop samples might be affected by some weathering or diagenetic overprinting and therefore it cannot be guaranteed that they represent conditions of the subsurface rocks. The majority of outcrops are located close to the Al Khawd dam and only two samples of the Barzaman Formation were taken at the southern foothills of the Oman Mountains (Lat. 22.3041702; Long. 57.8264319), where the former alluvial stream deposits form complex systems of 'raised' or upstanding, sinuous, superimposed linear ridges and broad gravel sheets (Maizels 1987). To correlate T-logs with physical rock properties, it was necessary to obtain rock samples from the same stratigraphic intervals. Therefore, our sampling strategy focused on the sediments encompassing the uppermost 700 m of the succession. In total we took 25 samples of the Barzaman Formation, the Ma'am reef sequence and the Seeb Formation. The thermal conductivity, effective porosity, permeability, and matrix density of each sample was determined. The rock thermal conductivity was measured with a thermal conductivity scanner (TCS, optical scanning technique). The underlying technique of the TCS has been described in detail by Popov et al. (1999). Samples were dried in an oven at 80 °C for 24 h before the thermal conductivity measurements were performed. A black acryl lacquer line was drawn on the polished and plain sample surface to avoid different mineral colors affecting the measurement. Additionally, we measured the thermal conductivity of water-saturated samples. For this, samples were saturated under vacuum in a desiccator for 3 days. The optical scanning technique is a transient method, which yields a continuous profile of thermal conductivity along the core axis of the sample. The mean thermal conductivity is determined as the arithmetic mean of all conductivities measured along the scanning line. To determine anisotropy measurements were made parallel and perpendicular to bedding planes, where developed.

Effective porosity and density of the rock samples were analyzed using the Archimedes method, which is based on the principle of mass displacement. Additionally, plugs of 25 mm diameter and 50 mm length were drilled for bulk permeability measurements. This was done using a conventional gas permeameter, and the results were adjusted with the Klinkenberg-correction method (Milsch et al. 2011), a procedure described in detail by Tanikawa and Shimamoto (2009). The sampled rocks comprise a range of different lithologies including: conglomerate, sandstone, limestone, mudstone, and siltstone and thus cover the major lithotypes comprising the shallow sedimentary cover of the Batinah coast.

### Temperature data

We analyzed temperature measurements of three wells (NB-1; NB-19; NB-22) located along the Batinah coast, to get a first approximation of the temperature pattern of the study area. The data were kindly provided by the Ministry of Regional Municipalities and Water Resources (MRMWR). These exploration wells are between 70 and 316 m



deep (cf. Fig. 4) and were drilled between 2005 and 2006 to evaluate the thickness, yield potential and water quality of the coastal aquifer. Additionally, litho-stratigraphic and gamma ray logs were available for these three wells.

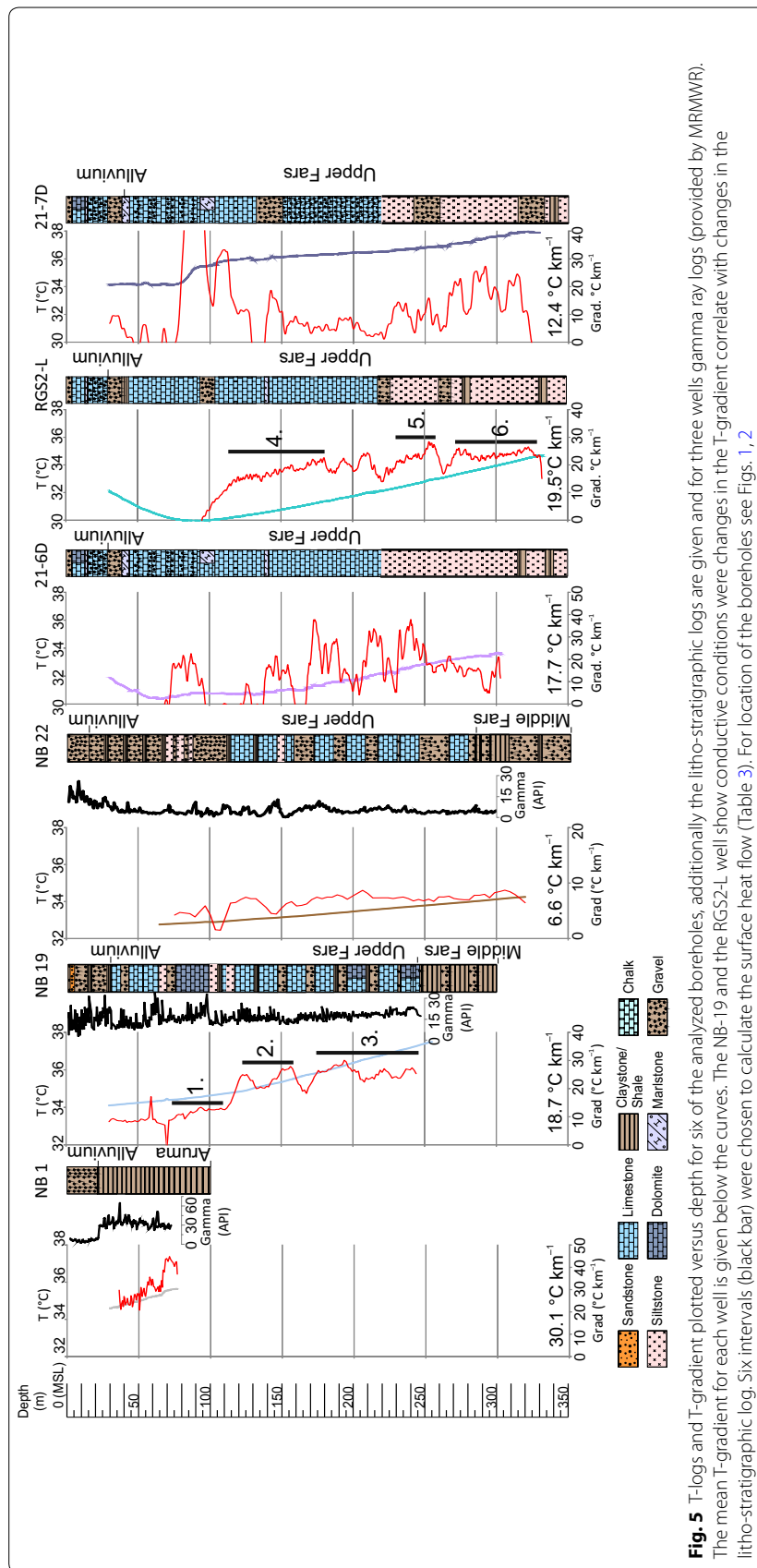
Our field campaign aimed to acquire additional high precision temperature data of existing water wells. The MRMWR provided a database with more than 300 boreholes, which were screened and evaluated as potential wells for temperature logging. The wells spread over the entire study area, but the deepest wells cluster around the Al Khawd dam, a recharge dam built in 1982 (see Fig. 2). The wells are mainly shallow (<100 m), only nine wells are deeper than 300 m and 35 wells are between 100 and 300 m. The wells exceeding 300 m in total depth were the main target for the temperature logging field campaign. Finally, seven wells were measured, five of which had a depth between 193 and 330 m, and two of them were only accessible to a depth of 90 and 45 m, respectively (Table 1). To identify the intervals in the T-logs that were measured above and below the water table it was important to know in advance in which depth the water level can be expected. For several wells the monitoring data of the water table were provided by the MRMWR. The data indicated that the water table around the Al Khawd dam varies between 20 and 30 m below ground level. The logging equipment consisted of a cable (500 m length), a conventional temperature probe and a mobile winch. The temperature probe was lowered to the borehole with the winch and lifted with a constant velocity of 3 m min<sup>-1</sup>. Thereby it measured a temperature point every 10 cm, resulting in a spatial continuous T-log. The slow speed guaranteed that turbulences affecting the measurements were kept as low as possible. Subsequently, the T-logs were smoothed with a 10 m running average (arithmetic mean). The results are plotted for all wells (temperature vs. depth) in Fig. 4 in combination with the data provided by the MRMWR. All ten wells are either exploration or monitoring wells, and are not used to produce water.

#### **Temperature gradient and surface heat flow**

For six wells litho-stratigraphic logs were available (NB-1, NB-19, NB-22, 21-6D, 21-7D, RGS2-L), and based on the T-logs we calculated the T-gradient for these six wells (cf. Fig. 5). A mean T-gradient is given for each of the well. For the calculation the negative T-gradient values of the shallow intervals were disregarded, as they do not represent steady state conditions. The T-gradient is plotted next to the litho-stratigraphic log to correlate changes in the lithological composition with changes in the T-gradient. If available gamma ray logs were also plotted. The T-logs from the two deepest wells, which show no significant advective component (NB-19, RGS2-L), were chosen for analysis of

**Table 1 Coordinates, completion date and total depth of wells, which were used for T-logging and wells of which T-logs were provided by the MRMWR (NB-1, NB-22, NB-19)**

ID	Coord. Y WGS	Coord. X WGS	Completion date	Total depth (m)
21-7D	23.6249	58.1887	1995-04-10	326
RGS-2L	23.6487	58.1659	1984-09-15	330
MAN-3	23.6306	58.0889	2012-01-12	300
21-6D	23.6385	58.1523	1995-04-10	300
RGS-5HS	23.6608	58.1747	1985-02-01	193
103	23.5804	58.1716	Unknown	90
SAG-13	23.6338	58.1804	1993-12-14	45
NB-1	24.7227	56.4159	2005-10-01	70
NB-22	23.6969	57.3677	2006-06-03	316
NB-19	23.7814	57.2416	2006-05-03	256



the surface heat flow. This facilitates the overall understanding of the conductive temperature pattern of the region. For this reason, the interval method was applied. This method is described by Powell et al. (1988) and has been applied successfully in recent heat flow studies (Förster et al. 2007; Schütz et al. 2014). The underlying principle is to identify intervals where changes in the T-gradient are clearly related to changes in the lithology, and hence changes in the thermal conductivity of the interval. The heat flow is defined by the Fourier equation:

$$q = -\lambda \cdot \Gamma, \quad (1)$$

where  $\lambda$  is the thermal conductivity ( $\text{W m}^{-1} \text{K}^{-1}$ ) and  $\Gamma$  is the T-gradient ( $\text{K km}^{-1}$ ) for the interval. For the two well locations we calculated mean heat flow values from the interval heat flow values.

## Results

### Physical rock properties

The thermal conductivity of the water-saturated rock samples ranges from 1.7 to  $2.9 \text{ W m}^{-1} \text{K}^{-1}$ . The Barzaman conglomerates show the lowest values ( $1.7\text{--}1.9 \text{ W m}^{-1} \text{K}^{-1}$ ), and fossiliferous limestone the highest ones ( $2.4\text{--}2.7 \text{ W m}^{-1} \text{K}^{-1}$ ). No effect of anisotropy was determined, therefore only the results of the measurements perpendicular to the bedding are shown in Table 2. The difference between dry and water-saturated samples is relatively small. The thermal conductivity of dry rock samples ( $\lambda_{\text{dry}}$ ) ranges from 0.9 to  $2.7 \text{ W m}^{-1} \text{K}^{-1}$  and the ratio of thermal conductivity measured on dry versus saturated samples ( $\lambda_{\text{dry}}$  vs.  $\lambda_{\text{sat}}$ ) ranges from 0.4 to 1.0 (mean value of 0.8) and is directly linked to the effective rock porosity. The carbonates reveal a relatively small difference between dry and water-saturated thermal conductivity values due to the little effective rock porosity. Very dense grainstones of the Ma'am reef sequence show slightly higher thermal conductivity values (mean  $\lambda_{\text{sat}} 2.8 \text{ W m}^{-1} \text{K}^{-1}$ ) than the less dense, mixed carbonate siliciclastic rocks of the Barzaman Formation (mean  $\lambda_{\text{sat}} 2.3 \text{ W m}^{-1} \text{K}^{-1}$ ). Effective porosity ranges between 1.1 and 36.3%, and is highest in the sandstones and sandy limestone samples. The sediments of the Seeb Formation deposited in a carbonate ramp system show a wide range of effective porosity values (2.2–33.8%, mean 16.8%). The main lithologies in the Seeb Formation are *Nummulites* grainstones/packstones at the base and wackestone to mudstones in the upper half of the sequence. The highest effective porosity can be found in the *Nummulite* grainstones/packstones and sandy limestones, which is in accordance with observations made in other regions. The *Nummulite limestone* of the Seeb Formation are excellent hydrocarbon reservoirs (e.g., Tunisia and Libya, Beavington-Penney et al. 2008) due to the high effective porosity and permeability. The lowest effective porosity values are observed in the Ma'am reef sequence (range 1.1–4.0%, mean 2.6%). The investigated section represents the main reef-top, which generally has a high effective porosity but was here probably affected by later diagenesis. The coarse-grained clastics of the alluvial fan system (Barzaman Formation) show a smaller range in effective porosity but a higher mean value (8.9–36.3%, mean 17.1%) than the Seeb Formation. Bulk permeability ranges between 0.01 and 7.5 mD, with highest values in the sandstones of the Seeb Formation (Table 2).

**Table 2 Overview of the sampled rocks with the lithology, geological formation, measured porosity ( $\varphi$ , %), density ( $\rho$ ,  $10^3 \text{ kg m}^{-3}$ ), permeability ( $k$ ,  $D$ ), the thermal conductivity measured on dry ( $\lambda_{\text{mean}_{\text{dry}}}$ ) and water-saturated ( $\lambda_{\text{mean}_{\text{sat}}}$ ,  $\text{W m}^{-1} \text{K}^{-1}$ ) samples**

Sample ID	Sample point	Lithology	Geological formation	$\varphi$ (%)	$\rho$ ( $\text{g cm}^{-3}$ )	$k$ [ $D$ ]	$\lambda_{\text{mean}_{\text{dry}}}$ ( $\text{W m}^{-1} \text{K}^{-1}$ )	$\lambda_{\text{mean}_{\text{sat}}}$ ( $\text{W m}^{-1} \text{K}^{-1}$ )
B1	x	Conglomerate, diagenetic alteration	Barzaman	17.0	2.2		1.79	1.90
B2	x	Conglomerate, diagenetic alteration	Barzaman	15.0	2.1		2.13	2.38
B3	3	Brownish pebbly sandstone	Barzaman	21.3	2.1	2.00E-04	1.56	2.28
B4	3	Sandy pebbly conglomerate	Barzaman	12.4	2.3	1.00E-05	2.24	2.50
B5	3	Coarse sized sandstone	Barzaman			3.50E-03	1.11	
B6	3	V.C sandstone	Barzaman	36.3	1.7	7.50E-03	0.74	1.93
B7	3	Limestone with pebble size clasts	Barzaman	21.2	2.1	1.00E-04	1.65	2.14
B8	3	Limestone (reef limestone)	Barzaman	14.6	2.3	6.00E-04	2.42	2.89
B9	3	Limestone breccia	Barzaman	12.8	2.3	8.00E-06	2.04	2.26
B10	3	Siltstone, partially cong	Barzaman	18.6	2.1		1.65	1.97
B11	3	Mudstone, beige	Barzaman				0.93	
B12	3	Polymictic conglomerate	Barzaman	18.6	2.1	6.00E-04	1.36	1.73
B13	3	Fossiliferous limestone	Barzaman	8.9	2.5	–	2.36	2.49
B14	3	Grainstone	Barzaman	10.0	2.4		2.27	2.49
B15	2	Conglomerate, diagenetic alteration	Barzaman	15.0	2.2	2.00E-04	2.27	2.72
MAM1	4	Limestone	MAM reef	2.5	2.6		2.71	2.80
MAM2	4	Fossiliferous-rich grainstone	MAM reef	1.1	2.7		2.64	2.71
MAM3	4	Fossiliferous-rich grainstone	MAM reef	4.0	2.6	–	2.63	2.76

**Table 2 (continued)**

Sample ID	Sample point	Lithology	Geological formation	$\varphi$ (%)	$\rho$ (g cm <sup>-3</sup> )	$k$ [D]	$\lambda_{\text{mean,dry}}$ (W m <sup>-1</sup> K <sup>-1</sup> )	$\lambda_{\text{mean,sat}}$ (W m <sup>-1</sup> K <sup>-1</sup> )
S1	5	Foraminiferal packstone-wackstone	Seeb	32.3	1.8	2.00E-04	1.09	1.83
S2	5	Foraminiferal grainstone	Seeb	8.8	2.5		2.15	2.42
S3	4	Foraminiferal packstone-wackstone	Seeb	33.8	1.8	3.80E-03	0.94	1.87
S4	1	Sandstone (sandy limestone)	Seeb	2.2	2.6		2.59	2.65
S5	4	Foraminiferal limestone	Seeb	7.2	2.5		2.35	2.73

Sampling points can be found in Fig. 2, B1 and B2 are not on the map

### Temperature data

The T-log of the RGS2L well shows decrease in temperature from 10 m (33.3 °C) to 95 m (30.0 °C) (Fig. 4). This is followed by a relatively smooth and homogeneous increase to the total depth (332 m, 34.6 °C). The temperature in the 21-6 D well shows a similar overall pattern. Between 83 m and 138 m the temperature remains relatively stable, followed by an increase from 30.7 to 33.7 °C and a final temperature of 33.5 °C at the total depth. However, at some depths a high noise is evident. Bodri and Cermak (2011) suggest that sharp discontinuities in a temperature-depth profile (so called “spike” anomalies) may reflect the in- and/or outflow of fluid and its movement within the borehole as well as groundwater flow along a fault or narrow horizontal layer. Transient signals from drilling and mud circulation process can be excluded as the well was completed long in the past (Table 1). The temperature curve in the RGS5HS well generally shows a similar trend as the previously described logs, but with overall slightly higher values and a minor temperature increase from 31.3 °C at 50 m to 32.3 °C at 197.5 m. The T-logs of the wells close to the shoreline show a strong decrease in the temperature in the first tens of meters. The RGS5HS well is located 2.65 km away from the shoreline and the temperature decreases from 32.9 °C at 13 m depth to 31.2 °C at 60 m depth. The subsequent temperature rise is almost negligible (~ 1.1 °C down to the final well depth of 198 m). The data of the 21-7D well show anomalous temperatures. After an increase in the first meters the temperature remains static to a depth of 80 m and then increases first abruptly and afterwards more gradually to 37.8 °C at the total depth of 330 m. As in the well 21-6D a certain noise is observed over the whole length of the log, the source is unknown. The wells were measured at the first (21-7D) and the fourth day (21-6D) of the field campaign with smooth and undisturbed measurements in between (RGS2L). However, a problem with the power unit cannot be ruled out. Background noise might have been generated by a dysfunctional wavelet generator. The temperature pattern of

the MAN-3 T-log is also disturbed. After an increase until a depth of 30 m no further temperature increase is observed to the total depth (300 m, 34.0 °C). This might indicate that the temperature probe was blocked by an obstacle. However, determination of such an outage at the surface is problematic. To avoid jamming of the probe, we attached a weight of 5 kg to the cable to ensure continuous downhole logging. This technique was also applied during this measurement, but gave no clear result at the bottom of the hole. A similar observation was made for the T-log of the SAG-13 well. The T-log of the well 103 is plotted only between 20 and 90 m, the shallower part was not considered due to extremely low temperatures. At 90 m the well was blocked. The temperature curve shows a very similar trend like the one of RGS2-L well. In the NB-22 well the water table is at 60 m depth, the temperature data are only given for the interval below the water table. The temperature curve shows a very smooth and minor temperature increase from 32.8 °C at 65 m depth to 34.3 °C at 320 m depth. The water table in the NB-19 well is recorded in 30 m depth, also here the T-logs starts below the water table. The temperature increase with depth is more significant in this borehole. The temperature rises from 34.1 °C at 30 m depth to 37.5 at 255 m depth. The temperature pattern shows no disturbance by advective flow. The temperature curve of the NB-1 well shows first an abrupt and then a moderate increase from 33.6 to 35.6 °C.

There is a notable temperature minimum between 50 and 90 m at the four well locations that are located closest to the shoreline (21-6D, RGS2L, RGS5HS, 103). The bottom-hole temperatures that were measured in a cluster of nine water wells close to the Al Khwad dam show a range of 30.0–33.0 °C at depth between 72 and 148 m. The results are plotted for all wells (temperature vs. depth) in Fig. 4 in combination with the data provided by the MRMWR.

### **Temperature gradient**

For six well locations the T-log and the calculated T-gradient are plotted next to the litho-stratigraphic log and gamma ray logs (Fig. 5). The calculated mean T-gradient for each of the six wells show a relatively large spread (6.6–30.1 °C km<sup>-1</sup>). T-gradients down to 30 m were disregarded as these are influenced by annual climate effects. Four wells (NB-19, 21-6D, 103, RGS5HS) show disturbances also in deeper parts or even over the whole logging interval. The T-gradient of the NB-22 well is anomalously low (mean 6.6 °C km<sup>-1</sup>) without any correlation to changes in the lithology. The T-gradient of the 21-6D well fluctuates strongly within small intervals, which is an indication for advective flow. The same observations can be made in the 21-7D well, which shows significant temperature perturbations between 80 and 110 m. In the conglomeratic limestone interval of the Upper Fars Group (155 and 200 m) the T-gradient is very low (~8 °C km<sup>-1</sup>). In the lowermost interval which consists of siltstone and claystone the T-gradient shows strong fluctuations around a mean of 18 °C km<sup>-1</sup>. The T-gradient of the NB-1 well is comparatively high with a mean of 30.1 °C km<sup>-1</sup>. This could be a result of the low thermal conductivity of the claystone which dominates this interval. However, the T-log covers only 50 m and hence it is not possible to achieve reliable results. The T-gradient of wells NB-19 and RGS2L seem to reflect a thermal equilibrium as changes can be



correlated to the lithology. Therefore, these two sites were chosen for a surface heat flow calculation.

### Surface heat flow

The T-gradient of the NB-19 well shows two peaks at 60 and 70 m depth which cannot be explained by changes in the lithology. Below these peaks the gradient seems undisturbed and three intervals were chosen for a surface heat flow calculation (see black bars in Fig. 5). The first interval is mainly composed of dolomite, with a slightly higher thermal conductivity ( $2.6 \text{ W m}^{-1} \text{ K}^{-1}$ ) value and a mean T-gradient of  $11.0 \text{ }^\circ\text{C km}^{-1}$  (Table 3). The second interval is composed of limestone, conglomerate and some shale and the T-gradient is significantly higher ( $23.0 \text{ }^\circ\text{C km}^{-1}$ ). The thermal conductivity was calculated based on the percentages of different lithotypes making up the depth interval and the corresponding thermal conductivity values from Table 2. The third interval consists of conglomerates limestone and minor chalk, shale and dolomitic limestone. This results in a mean T-gradient of  $24.0 \text{ }^\circ\text{C km}^{-1}$  and a mean thermal conductivity of  $2.4 \text{ W m}^{-1} \text{ K}^{-1}$ . The interval surface heat flow values range between 28.6 and  $57.6 \text{ mW m}^{-2}$  with a mean of  $47.9 \text{ mW m}^{-2}$ . In the RGS2-L well an undisturbed T-gradient can be identified below 100 m. Three interval T-gradients corresponding to lithological changes are marked by a black bar (Fig. 5). In between these intervals minor disturbances occur, which are not reflected in the litho-stratigraphic log. The first interval is dominated by limestone (mean T-gradient  $18 \text{ }^\circ\text{C km}^{-1}$ , mean thermal conductivity  $2.5 \text{ W m}^{-1} \text{ K}^{-1}$ ) and the interval surface heat flow is  $45.0 \text{ mW m}^{-2}$ . The second interval is mainly dominated by siltstone, reflected in a relatively low mean thermal conductivity ( $2.2 \text{ W m}^{-1} \text{ K}^{-1}$ ) and a slightly higher T-gradient compared to the shallower interval ( $23.0 \text{ }^\circ\text{C km}^{-1}$ ). The lowermost interval is comparable to the one described before. The litho-stratigraphic log indicates shale in addition to the siltstone, which results in slightly lower thermal conductivity values but a constant T-gradient. The interval surface heat flow values range from 44.0 to  $50.1 \text{ mW m}^{-2}$  the mean value is  $46.4 \text{ mW m}^{-2}$ .

### Implication for temperature predictions

The determined surface heat flow can be used to calculate the temperature at depth beyond the logging depth. Knowledge of the sedimentary infill of the basin is required for such an analysis to be able to estimate thermal conductivity data for the different

**Table 3 Surface heat flow calculation with the interval method for two well locations**

Well	Interval		$\Gamma$ ( $^\circ\text{C km}^{-1}$ )	Lith.	$\lambda$ ( $\text{W m}^{-1} \text{ K}^{-1}$ )	$q_{\text{interval}}$ ( $\text{mW m}^{-2}$ )	$q_{\text{mean}}$ ( $\text{mW m}^{-2}$ )
	Nr.	(m)					
NB-19	1	74–109	11.0	Dol.	2.6	28.6	47.9
	2	122–158	23.0	Ls. Cong.	2.5	57.5	
	3	174–245	24.0	Ls. Cong. Dol.	2.4	57.6	
RGS2-L	4	112–180	18.0	Ls	2.5	45.0	46.4
	5	230–267	23.0	Si.	2.2	50.1	
	6	271–329	22.0	Si.	2.0	44.0	

The intervals are marked with a black bar in Fig. 5. For location of the wells see Fig. 2. The interval gradient ( $\Gamma$ ) is given in  $^\circ\text{C km}^{-1}$ , major lithological units of the interval are given (lith.), interval thermal conductivity ( $\lambda$ ) is given in  $\text{W m}^{-1} \text{ K}^{-1}$ . Interval surface heat flow ( $q_{\text{interval}}$ ) and mean surface heat flow ( $q_{\text{mean}}$ ) are given in  $\text{mW m}^{-2}$

lithological layers. For this purpose we used litho-stratigraphic information from Nolan et al. (1990). We estimated the thermal conductivity of stratigraphic formations by taking the proportion of different rock types into account. We used mean thermal conductivity data determined in this study, for the shallow sedimentary formations (Alluvial, Barzaman Fm., Ma'am reef sequence, Seeb Fm.). For rock types, not measured in this study, we used literature data (Norden and Förster 2006; Fuchs and Förster 2010). The Al Khawd Formation is composed of conglomerates and sandstones and a thermal conductivity of 3.2 is assumed (Beach et al. 1986; Norden and Förster 2006). The Simsima Formation is composed of bioclastic limestone; therefore, we assigned a thermal conductivity of  $2.7 \text{ W m}^{-1} \text{ K}^{-1}$ , typical for limestone (Schütz et al. 2012). Below follows the Semail Ophiolite complex consisting of basalt and gabbro with a thermal conductivity of  $2.2 \text{ W m}^{-1} \text{ K}^{-1}$  (Norden and Förster 2006). The thickness of the stratigraphic formations derives from Nolan et al. (1990), however, the depth of the transition from the post-obduction sediments to the ophiolites is not yet determined with certainty. The temperature at depth is calculated (based on the Fourier equation) by summing the results of the incremental temperature calculations across individual layers of uniform conductivity:

$$T_z = T_s + \sum_i^n \left[ z_i \frac{q_s}{\lambda_i} \right] \quad (2)$$

where  $T_s$  (K) and  $q_s$  ( $\text{mW m}^{-2}$ ) are the temperature and heat flow at the surface,  $z_i$  is the thickness and  $\lambda_i$  ( $\text{W m}^{-1} \text{ K}^{-1}$ ) is the thermal conductivity of unit  $i$ . An annual average surface temperature of  $29 \text{ }^\circ\text{C}$  and two different values of surface heat flow ( $46$  and  $48 \text{ mW m}^{-2}$ ) are used. Pressure correction was performed of the thermal conductivity to reflect the in situ pressure conditions with the following equation (Fuchs and Förster 2013):

$$\lambda_{p,\text{cor}} = (1.095 \cdot \lambda_{\text{lab}} - 0.172) \cdot p^{(0.0088 \cdot \lambda_{\text{lab}} - 0.0067)}, \quad (3)$$

where  $\lambda_{\text{lab}}$  ( $\text{W m}^{-1} \text{ K}^{-1}$ ) is the thermal conductivity determined in the lab with zero pressure and  $p$  (MPa) is the assumed in situ pressure.

To correct the thermal conductivity to the expected in situ temperature the approach of Somerton (1992) was used:

$$\lambda_{T,\text{cor}} = \lambda_{20} - 10^{-3}(T - 293) \cdot (\lambda_{20} - 1.38) \cdot \left[ \lambda_{20}(1.8 \cdot 10^{-3} T)^{-0.25\lambda_{20}} + 1.28 \right] \lambda_{20}^{-0.67}, \quad (4)$$

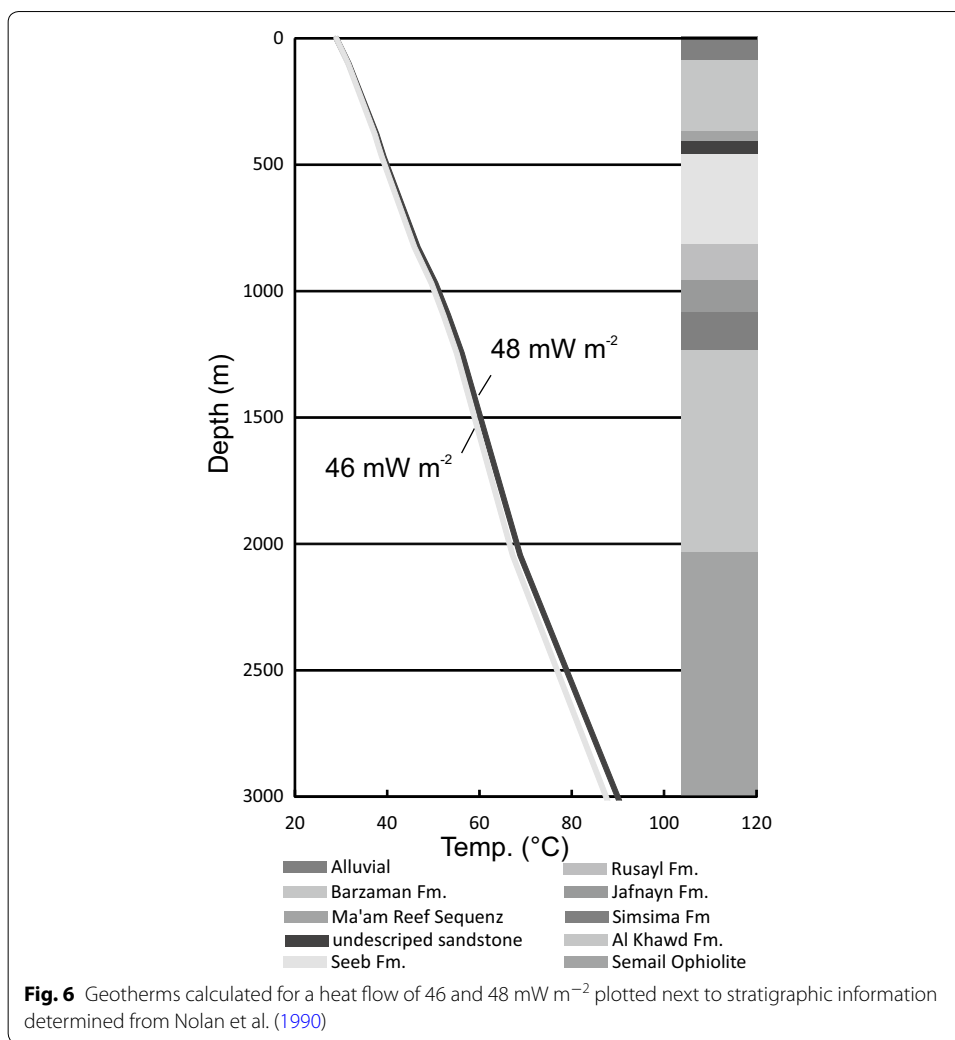
where  $\lambda_{20}$  ( $\text{W m}^{-1} \text{ K}^{-1}$ ) is the thermal conductivity at  $20 \text{ }^\circ\text{C}$  and  $T$  (K) is the expected in situ temperature.

The results of the temperature at depth calculation are plotted in Fig. 6.

## Discussion

### Physical rock properties

The rock properties determined in this study give first insights in the thermal characteristics of the sedimentary rocks in the foreland basin of northern Oman. The thermal conductivities of the rocks are moderate without any significant high values.



Only a mudstone from the Barzaman Formation shows noticeable low values (mean  $0.9 \text{ W m}^{-1} \text{ K}^{-1}$ ). The effective porosities and permeabilities are the controlling parameters for the type of geothermal energy usage. Sedimentary layers with high effective porosity and permeability values in principle allow hydrothermal exploitation of the system, whereas very tight sedimentary rocks require additional stimulation to enhance hydraulic performance (Enhanced Geothermal Systems, EGS). Although some sandstone samples from the Seeb Formation and the Barzaman Formation show a high effective porosity (32.3–36.3%) the corresponding permeability values are low ( $2.0 \times 10^{-4}$ – $7.5 \times 10^{-3}$  mD). This indicates that the measured porosity is not only reflecting effective porosity, but also ineffective porosity, which is in contradiction to values that have been determined on rock samples from the equivalent sedimentary formation from Tunisia (Beavington-Penney et al. 2008). We determined the physical rock properties that only represent the shallow sedimentary cover (< 700 m, depth of the Seeb Formation). These data are important for the planning of shallow geothermal systems like aquifer thermal energy storage or heat sinks to dispense process waste heat to the underground, especially if no appraisal wells exist. The thermal conductivity also cannot

be determined through downhole geophysics. More accurate data could only be determined if measurements were carried out on core samples. Another option is to determine the thermal conductivity indirectly by use of different petrophysical logs (Fuchs et al. 2015). Winterleitner et al. 2018 used the database presented here as the basis for a study on the impact of subsurface heterogeneities on high-temperature aquifer thermal energy storage systems for northern Oman. To understand the deeper parts of the foreland basin and to calculate the temperature at depth beyond logging data the thermal conductivities were interpolated to depth based on litho-stratigraphic information from Nolan et al. 1990 (cf. “[Implication for temperature predictions](#)” section). Temperature and pressure impacts on the thermal conductivity were considered. The effect of pressure seems to be slightly higher, which results in an overall higher temperature of 143.4 °C in 4631 m depth compared to 139.4 °C when no pressure correction is applied (for the case of 48 mW m<sup>-2</sup>). However, the two effects basically cancel each other out.

#### **Subsurface temperature distribution in the study area**

In general, the determined temperature pattern of the ten wells is relatively consistent (Fig. 4). In all cases, the temperature curves show higher temperatures down to ~30 m. This reflects a response of soil and bedrock to warming from the atmosphere. The first tens of meters of the temperature profiles are clearly not representing steady state conditions, but are disturbed by advective flow of heat. A reconstruction of the undisturbed geothermal gradient would be possible if satisfactory hydrological information of the area were available, especially the groundwater flow. Further, the southern Batinah coast is affected by saltwater intrusion into the coastal aquifer system due to excessive groundwater withdrawal for irrigated agriculture (Walther et al. 2012; Grundmann et al. 2014; Chitrakar and Sana 2016). This might be reflected in negative temperature gradients close to the sea in the first tens of meters after the climate related temperature peak. However, no significant decrease in groundwater elevation has been reported around the Al Khawd dam (MRMW, cf. Fig. 3) and therefore the negative temperature gradients might also reflect advective fluid flow related to topography.

The temperature gradient is comparable low along the Batinah coast (Fig. 5) with a mean temperature gradient of around 17.5 °C km<sup>-1</sup> for the six wells plotted in Fig. 5. However, only two of the six wells with litho-stratigraphic log correlation show undisturbed conditions and seem to be under a thermal equilibrium (NB-19, RGS2-L) with a mean temperature gradient of 19.1 °C km<sup>-1</sup>. It is likely that a relatively low temperature gradient is representative for the Batinah coast, even if advective disturbance is present in the shallow intervals of the wells. This is in accordance with T-gradients determined by Rolandone et al. (2013) in 13 water wells (6.6–26.1 °C km<sup>-1</sup>) in south and north Oman. The closest water wells that were analyzed by the authors are in the northern Batinah coast around 230 km to the northwest of our study area. In two water wells the authors determined T-gradients of 6.6 and 11.6 °C km<sup>-1</sup>, but only the higher value is considered to be reliable.

The target temperature for geothermal exploitation is 70–100 °C, if the heat is to be used to drive an absorption chiller or for water desalinization. When the annual average surface temperature of Muscat (29 °C) is applied the target temperatures can be calculated using the determined surface heat flow and the thermal conductivity of

stratigraphic formations as model input. This results in a target depth of about 2000–3000 m (Fig. 6). The use of geothermal energy in the sedimentary section would be possible, but only in the deeper parts of the foreland basin.

Besides suitable hydraulic properties the rejection of process waste heat to the underground requires stable and low temperatures. The temperature logs give an idea which depth levels might be considered for such an application. Varying between 29.9 and 34.4 °C the temperature logs show a minimum between 50 and 100 m depth. These values are only slightly above the average annual surface temperature of Muscat (29 °C), and significantly lower than peak temperatures during summer time (47 °C) and therefore constitute a suitable target for rejecting process waste heat.

#### **Surface heat flow of the Arabian Platform**

Rolandone et al. (2013) determined a uniformly low ( $45 \text{ mW m}^{-2}$ ) surface heat flow in the entire region of the eastern Arabian Platform, which is in accordance with the results determined from the newly measured temperature profiles of this study. Determination of the surface heat flow of two selected boreholes resulted in values of 46.4 and  $47.9 \text{ mW m}^{-2}$  with a mean of  $47.2 \text{ mW m}^{-2}$ . However, if such low values are representative for all Oman is a question which has to be solved by a broader heat flow study. The determination of heat flow values for the Batinah coast allows the generation of 2D or 3D thermal models of the sedimentary basin. The basis for such a model would be a geological model incorporating all the major geological units. The required input parameters that need to be assigned to each geological unit are the thermal conductivity, the radiogenic heat production and the density. The heat flow then constitutes the boundary condition, together with the annual surface temperature. Such a model would allow the generation of temperature-depth maps. The radiogenic heat production of the sedimentary cover can contribute significantly to the surface heat flow when clastic sediments are dominant. In case of the neoautochthonous sedimentary cover the amount of radiogenic heat production is probably minor due to the prevalence of carbonates. This is also reflected in several gamma ray logs provided by the MRMWR. The logs are recorded in API units and among six well logs the values are below 50 API with a mean of 15 API (cf. Fig. 5), which is characteristic for carbonatic dominated composition (Vila et al. 2010).

#### **Conclusions**

Newly measured temperature logs of six well locations and the three T-logs provided by the MRMW were used as a basis to calculate the geothermal gradient of the Batinah coast. The calculation indicates a relatively low geothermal gradient ( $\sim 19.1 \text{ }^\circ\text{C km}^{-1}$ ), and a temperature window of 70–90 °C reached at 2000–3000 m depth (Fig. 6). The results show that geothermal energy as heat source for a thermally driven absorption chiller is an option even in areas with low geothermal gradients. The required temperatures are reached in a drillable depth within the sedimentary basin. Geothermal energy can significantly contribute to cover the base load of such a cooling system that is not available through solar thermal energy. With geothermal energy as heat source for a thermally driven cooling system a storage system would become less relevant. Whereas, it is vital when a fluctuating heat source, like the sun, is used. To further evaluate the geothermal potential of the study area it is crucial to

carry out structural analysis. Especially the hot springs in the area indicate a potential geothermal target. At one spring a temperature of 66 °C was measured (data provided by the MRMWR); it is located where the post-nappes sedimentary deposits have been faulted against the autochthonous series. Fournier et al. 2006 reconstructed the local stress tensor and identified two phases of extension followed by a compressional phase. The authors analyzed fractures on outcrop scale which could be used to understand the hydraulic behavior of the faults. Therefore, a coupled heat and fluid transport analysis is required to better understand the potential of fault/fracture controlled geothermal activity in the study area.

The surface heat flow calculated for two sites show relatively low values (47.9 and 46.4 mW m<sup>-2</sup>). Such low heat flow values have been determined at different sites in Oman (Rolandone et al. 2013) but are nevertheless atypical for the crustal setting. Heat-flow values in the middle and upper 50 mW m<sup>-2</sup> are determined in other regions for provinces of Neoproterozoic age (Nyblade and Pollack 1993; Rudnick et al. 1998). A crustal transect generated from seismic data (Al-Lazki and Barazangi 2002) indicates a Moho depth of about 40 km under the passive continental margin of north-eastern Oman. The metamorphic basement is around 25 km thick, and the average thickness of the sedimentary cover is around 15 km. In this study a transition from the upper to the lower crust (Conrad discontinuity) is not indicated. The upper crust consists of the sedimentary cover, metamorphic rocks and granites/granodiorites, whereas the lower crust is defined by a more mafic composition with plagioclase-rich and pyroxenite-rich granulite. Assuming a normal heat flow at the Moho ( $q_m = 25 \text{ mW m}^{-2}$ , Artemieva and Mooney 2001) and moderate radiogenic heat production in each of the crustal layers a surface heat flow of around 58 mW m<sup>-2</sup> would be expected. Thus, the surface heat flow determined in the present and previous study (Rolandone et al. 2013) are around 10 mW m<sup>-2</sup> lower, than the crustal setting would imply. Further studies on the crustal heat flow of the Arabian Peninsula in general, and Oman in particular are essential to better understand the temperature pattern of the broader region.

The temperature gradient, surface heat flow and thermal properties determined in this study serve as input parameter for simulations of the underground to plan potential shallow geothermal applications. Knowledge of the temperature distribution in the subsurface and the physical rock properties is fundamental in the development of underground storage system. The rejection of process waste heat to the underground is a relevant topic for the whole Arabian Peninsula, where temperatures during summer can reach more than 47 °C (in Muscat, PACA) causing all conventional technologies to be either inefficient or expensive. A stable temperature below 35 °C is required to efficiently reject process waste heat of an absorption chiller. The temperature logs of this study suggest temperatures that would be sufficient to reject the heat into the ground. Minimum temperatures (~ 30 °C) were measured between 50 and 100 m at the four well locations located closest to the shoreline (21-6D, RGS2L, RGS5HS, 103) and these temperatures are significantly lower than the maximum temperatures that can be reached during the hottest month. Due to the low temperature gradient deeper parts of the basin might also be suitable. Only three of the ten T-logs show temperatures > 35 °C (21-7D, NB-19, NB-1).

**Authors' contributions**

FS carried out the field work and developed the results. FS also drafted the manuscript. The second and third authors, GW and EH, supervised the research and guided the interpretation of results. GW and EH also considerably edited and improved the drafts. GW advised the geological field work and gave technical support during the data acquisition process. All authors read and approved the final manuscript.

**Author details**

<sup>1</sup> Section 6.2 Geothermal Energy Systems, Helmholtz Centre Potsdam-GFZ German Research Centre for Geoscience, Telegrafenberg, 14473 Potsdam, Germany. <sup>2</sup> Department for Earth and Environmental Sciences, University of Potsdam, Karl-Liebknecht Straße 24-25, Golm, Germany.

**Acknowledgements**

We particularly wish to thank the Ministry of Regional Municipalities and Water Resources for granting permission for the use of wells, data and their library. We would like to thank Hilal Al Julandani and Musaab Al Sarmi (SQU) for logistic support and assistance in the field work as well as Ronny Giese and Tanja Ballerstedt (GFZ). Christian Wenzlaff (GFZ) is thanked for his support in the lab. The manuscript profited from valuable remarks by two anonymous referees and Christina von Nicolai.

**Competing interests**

The authors declare that they have no competing interests.

**Availability of data and materials**

They are included in the publication. Raw data are not applicable.

**Consent for publication**

Not applicable.

**Ethics approval and consent to participate**

Not applicable.

**Funding**

The study is funded through Institute of Advanced Technology Integration (IATI)/The Research Council of the Sultanate of Oman and part of the GeoSolCool-project (<https://www.gfz-potsdam.de/en/section/geothermal-energy-systems/projects/geosolcool/>).

**Publisher's Note**

Springer Nature remains neutral with regard to jurisdictional claims in published maps and institutional affiliations.

Received: 11 October 2017 Accepted: 5 March 2018

Published online: 15 March 2018

**References**

- Al-Husseini M. Launch of the Middle East geologic time scale. *GeoArabia*. 2008;13(4):11, 185–8.
- Al-Lazki AI, Seber D, Sandvol E, Barazangi M. A crustal transect across the Oman Mountains on the eastern margin of Arabia. *GeoArabia*. 2002;7:47–78.
- Alsharhan AS. Petroleum systems in the Middle East. In: Rollinson HR, Searle MP, Abbasi IA, Al-Lazki A, Al Kindi MH, editors. *Tectonic evolution of the Oman Mountains*, vol. 392. London: Geological Society, Special Publications; 2014. p. 361–408.
- Artemieva IM, Mooney WD. The thermal thickness and evolution of pre-cambrian lithosphere: a global study. *J Geophys Res B*. 2001;106:16387–414.
- Beach RDW, Jones FW, Majorowicz JA. Heat flow and heat generation estimates for the Churchill basement of the Western Canadian Basin in Alberta, Canada. *Geothermics*. 1986;16(1):1–16.
- Beavington-Penney SJ, Nadin P, Wright VP, Clarke E, McQuilken J, Bailey HW. Reservoir quality variation on an Eocene carbonate ramp, El Garia formation, offshore Tunisia: structural control of burial corrosion and dolomitisation. *Sediment Geol*. 2008;209(1–4):42–57.
- Bodri L, Cermak V. Borehole climatology: a new method how to reconstruct climate. Amsterdam: Elsevier; 2011. p. 352.
- Breton J-P, Béchenec F, Le Métour J, Moen-Maurel L, Razin P. Eoalpine (Cretaceous) evolution of the Oman Tethyan continental margin: insights from a structural field study in Jabal Akhdar (Oman Mountains). *GeoArabia*. 2004;9(2):2004.
- Chang S-J, Van der Lee S. Mantle plumes and associated flow beneath Arabia and East Africa. *Earth Planet Sci Lett*. 2011;302:448–54.
- Chitrakar P, Sana A. Groundwater flow and solute transport simulation in Eastern Al Batinah Coastal Plain, Oman: case study. *J Hydrol Eng*. 2016;21(2):05015020.
- Coleman RG. Tectonic setting for ophiolite obduction in Oman. *J Geophys Res*. 1981;6(B4):2497–508.
- Dill HG, Wehner H, Kus J, Botz R, Berner Z, Stüben D, Al-Sayigh A. The Eocene Rusayl Formation, Oman, carbonaceous rocks in calcareous shelf sediments: environment of deposition, alteration and hydrocarbon potential. *Int J Coal Geol*. 2007;72(2):89–123.
- Förster A, Förster H-J, Masarweh R, Masri A, Tarawneh K. The surface heat flow of the Arabian Shield in Jordan. *J Asian Earth Sci*. 2007;30:271–84.
- Fournier M, Lepvrier C, Razin P, Jolivet L. Late cretaceous to paleogene post-obduction extension and subsequent Neogene compression in Oman Mountains. *GeoArabia*. 2006;11(4):17–40.



- Fuchs S, Förster A. Rock thermal conductivity of mesozoic geothermal aquifers in the Northeast German Basin. *Chem Erde*. 2010;70(Supplement 3):13–22.
- Fuchs S, Förster A. Well-log based prediction of thermal conductivity of sedimentary successions: a case study from the North German Basin. *Geophys J Int*. 2013;196:291–311.
- Fuchs S, Balling N, Förster A. Calculation of thermal conductivity, thermal diffusivity and specific heat capacity of sedimentary rocks using petrophysical well logs. *Geophys J Int*. 2015;203(3):1977–2000.
- GCC. The GCC in 2020: resources for the future. The Economist Intelligence Unit Limited; 2010.
- Grundmann J, Schütze N, Heck V. Optimal integrated management of groundwater resources and irrigated agriculture in arid coastal regions. Evolving water resources systems: understanding, predicting and managing water–society interactions. In: Proceedings of ICWRS2014, Bologna, Italy, June 2014 (IAHS Publ. 364, 2014). 2014.
- Huenges E, editor. Geothermal energy systems: exploration, development and utilization. Weinheim: Wiley-VCH; 2010.
- Johnson PR, Andresen A, Collins AS, Fowler AR, Fritz H, Ghebreab W, Kusky T, Stern RJ. Late Cryogenian-Ediacaran history of the Arabian–Nubian Shield: a review of depositional, plutonic, structural, and tectonic events in the closing stages of the northern East African Orogen. *J Afr Earth Sci*. 2011;61:167–232.
- Kusky T, Robinson C, El-Baz F. Tertiary-Quaternary faulting and uplift in the northern Oman Hajar mountains. *J Geol Soc*. 2005;162(5):871–88.
- Lashin A, Al-Arifi N, Chandrasekharan D, Al Bassam A, Rehman S, Pipan M. Geothermal energy resources of Saudi Arabia: country update. In: Proceedings World Geothermal Congress, Melbourne, Australia. 2015.
- Mahmoud S, Reilinger R, McClusky S, Vernant P, Tealeb A. GPS evidence for northward motion of the Sinai Block: implications for E, Mediterranean tectonics. *Earth Planet Sci Lett*. 2005;238:217–24.
- Maizels JK. Plio-Pleistocene raised channel systems of the western Sharqiyah (Wahiba), Oman. In: Frostick L, Reid I, editors. Desert sediments: ancient and modern, vol. 35. Geological Society, Special Publication: London; 1987. p. 31–50.
- Mann A, Hanna SS, Nolan SC, Mann A, Hanna SS. The post-campanian tectonic evolution of the Central Oman Mountains: tertiary extension of the Eastern Arabian Margin, vol. 49, no. 1. London: Geological Society, Special Publications; 1990. p. 549–63.
- Michard A, Bouchez JL, Ourzzani-Touhami M. Obduction related planar and linear fabrics in Oman. *J Struct Geol*. 1984;6:39–50.
- Milsch H, Priegnitz M, Blöcher G. Permeability of gypsum samples dehydrated in air. *Geophys Res Lett*. 2011;38:L18304.
- Mount VS, Crawford RIS, Bergman SC. Regional structural style of the central and southern Oman mountains: Jebel Akhdar, Saih Hatat, and the northern Ghaba Basin. *GeoArabia*. 1998;3:475–90.
- Nolan SC, Skelton PW, Clissold BP, Smewing JD. Maastrichtian to early tertiary stratigraphy and palaeogeography of the Central and Northern Oman Mountains, vol. 49, no. 1. London: Geological Society, Special Publications; 1990. p. 495–519.
- Norden B, Förster A. Thermal conductivity and radiogenic heat production of sedimentary and magmatic rocks in the Northeast German Basin. *AAPG Bull*. 2006;90(6):939–62.
- Nyblade AA, Pollack HN. A global analysis of heat flow from Precambrian terrains: implications for the thermal structure of Archean and proterozoic litho-sphere. *J Geophys Res B*. 1993;98:12207–18.
- Özcan E, Abbasi IA, Drobne K, Govindan A, Jovane L, Boukhalfa K. Early Eocene orthophragminids and alveolinids from the Jafnayn Formation, N Oman: significance of *Nemkovella stockari* Less & Özcan, 2007 in Tethys. *Geodin Acta*. 2015;28(3):160–84.
- Popov YA, Pribnow DFC, Sass JH, Williams CF, Burkhardt H. Characterization of rock thermal conductivity by high-resolution optical scanning. *Geothermics*. 1999;28:253–76.
- Poupeau G, Saddiqi O, Michard A, Goffé B, Oberhänsli R. Late thermal evolution of the Oman Mountains subophiolitic windows: apatite fission-track thermometry. *Geology*. 1998;26(12):1139–42.
- Powell WG, Chapman DS, Balling N, Beck AE. Continental heat flow density. In: Haenel R, Rybach L, Stegena L, editors. Handbook of terrestrial heat-flow density determination. Dordrecht: Kluwer; 1988. p. 167–222.
- Reiche D. Energy Policies of Gulf Cooperation Council (GCC) countries—possibilities and limitations of ecological modernization in rentier states. *Energy Policy*. 2010;38:2395–403.
- Rolandone F, Lucazeau F, Leroy S, Mareschal J-C, Jorand R, Goutorbe B, Bouquerel H. New heat flow measurements in Oman and the thermal state of the Arabian Shield and Platform. *Tectonophysics*. 2013;589:77–89.
- Rudnick RL, McDonough WF, O'Connell RJ. Thermal structure, thickness and composition of continental lithosphere. *Chem Geol*. 1998;145:395–411.
- Schütz F, Norden B, Förster A; DESIRE Group. Thermal properties of sediments in southern Israel: a comprehensive data set for heat flow and geothermal energy studies. *Basin Res*. 2012;24(3):357–76.
- Schütz F, Förster H-J, Förster A. Thermal conditions of the central Sinai Microplate inferred from new surface heat-flow values and continuous borehole temperature logging in central and southern Israel. *J Geodyn*. 2014;76:8–24.
- Searle MP. Sequence of thrusting and origin of culminations in the northern and central Oman Mountains. *J Struct Geol*. 1985;7:129–43.
- Searle MP, James NP, Calton TJ, Smewing JD. Sedimentological and structural evolution of the Arabian continental margin in the Musandam Mountains and Dibba Zone, United Arab Emirates. *Bull Geol Soc Am*. 1983;94:1381–400.
- Somerton WH. Thermal properties and temperature-related behavior of rock/fluid systems. Amsterdam: Elsevier Science Publishers B.V.; 1992. p. 257.
- Stern RJ, Johnson P. Continental lithosphere of the Arabian Plate: a geologic, petrologic, and geophysical synthesis. *Earth Sci Rev*. 2010;101:29–67.
- Sweetnam T, Al Ghaithi H, Almaskari B, Calder C, Patterson J, Mohaghedi S, Oreszczyzn T, Rasla R. Residential energy use in Oman: a scoping study. Project Report. 2014.
- Tanikawa W, Shimamoto T. Comparison of Klinkenberg-corrected gas permeability and water permeability in sedimentary rocks. *Int J Rock Mech Min*. 2009;46(2):229–38.
- Tomás S, Frijia G, Bömelburg E, Zamagni J, Perrin C, Mutti M. Evidence for seagrass meadows and their response to paleoenvironmental changes in the early Eocene (Jafnayn Formation, Wadi Bani Khalid, N Oman). *Sediment Geol*. 2016;341:189–202.



- Vila M, Fernández M, Jiménez-Munt I. Radiogenic heat production variability of some common lithological groups and its significance to lithospheric thermal modelling. *Tectonophysics*. 2010;490:152–64.
- Walther M, Delfs J-O, Grundmann J, Kolditz O, Liedl R. Saltwater intrusion modeling: verification and application to an agricultural coastal arid region in Oman. *J Comput Appl Math*. 2012;236(18):4798–809.
- Winterleitner G, Schütz F, Wenzlaff C, Huenges E. The impact of subsurface heterogeneities on high-temperature aquifer thermal energy storage systems. A case study from Northern Oman. *Geothermics*. 2018. (Accepted).

**Submit your manuscript to a SpringerOpen<sup>®</sup> journal and benefit from:**

- ▶ Convenient online submission
- ▶ Rigorous peer review
- ▶ Open access: articles freely available online
- ▶ High visibility within the field
- ▶ Retaining the copyright to your article

---

Submit your next manuscript at ▶ [springeropen.com](https://www.springeropen.com)

---